Annu. Rev. Biophys. Biophys. Chem. 1990. 19:267–99

MECHANISMS OF LONG-DISTANCE ELECTRON TRANSFER IN PROTEINS: Lessons from Photosynthetic Reaction Centers

Steven G. Boxer

Department of Chemistry, Stanford University, Stanford, California 94305

KEY WORDS: Stark spectroscopy, electric field effects, membrane proteins.

CONTENTS

PERSPECTIVES AND OVERVIEW

The movement of an electron from one redox active site to another is central to the function of many biological systems. Often, electron transfer reactions occur in series in an organized assembly of proteins. This situation arises in photosynthetic reaction centers as well as in many other

0883–9182/90/0610–0267$02.00

energy-transducing electron transport chains. The relevant biophysical issues I will address include the following: (*a*) How do electrons move over the substantial distances between redox active centers imposed by the bulk of the protein surrounding the active sites? (*b*) How do the distances between redox centers, the free energy change, and various aspects of solvation combine to determine the rate of electron transfer? (*c*) Is the role of the protein primarily structural, or do electronic states of the amino acid side chains and the peptide backbone modulate the rate of electron transfer? (*d*) Do fundamental differences separate electron transfer reactions in proteins from those in simpler solvents? (*e*) Do the parameters governing electron transfer between metal centers differ from those involving organic redox centers? (*f*) How are the movements of other charged particles, notably protons, coupled to the movement of electrons?

Although electron transport chains are commonly diagramed in introductory biochemistry and biophysics textbooks as ordered arrays of redox active proteins, there are relatively few structurally characterized examples of such arrays. The bacterial photosynthetic reaction center (RC) is a notable example. Researchers have determined the structures of RCs from several species in the past few years to atomic resolution using x-ray crystallography (1, 2, 24, 34, 35, 95). The structure of the *Rhodopseudomonas viridis* RC was the first membrane protein structure delineated (34) and is especially remarkable because it contains at least eight redox active sites covering a distance of more than 80 Å. A photon drives the initial charge separation step; further separation of the electron and hole occurs independently in a series of dark reactions. There is an extensive body of kinetic and thermodynamic data for each reaction, and in many cases one can study undesirable charge recombination reactions. The RC system is especially well suited for quantitative spectroscopic studies: the series of electron transfers is initiated with light; the neutral, anion, and cation spectra of many chromophores have been characterized; and the rates of many reactions are nearly independent of temperature. Remarkably, different electron transfer reactions, whose time constants range from about one picosecond up to tens of seconds, occur within this single chromophore-protein complex, enabling one to investigate examples of nearly all aspects of electron transfer dynamics.

Electron transfer is also a central process in chemistry and physics. Researchers have done a wealth of theoretical work, ranging from elementary theories of electron tunneling between potential wells (now a standard introductory quantum mechanics problem) to more sophisticated treatments that recognize the fundamental importance of changes in the position of the nuclear degrees of freedom that must be coupled to the movement of electrons (e.g. changes in bond length and the orientation of polar

solvent molecules). In the following, I sketch these theoretical treatments briefly because they provide both the vocabulary used in the field and a basis for interpreting experimental results. This discussion is necessarily oversimplified and is intended for the nonspecialist. The goal is to provide the basis for understanding the expected dependence of electron transfer rates on distance, driving force, temperature, and reorganization energy. A rather detailed analysis of current thinking on the mechanism of some of the electron transfer steps in the bacterial reaction center will follow. Then I will compare and contrast the RC work with studies of electron transfer in other protein-based systems.

ELECTRON TRANSFER THEORY

Several exceptionally useful reviews on electron transfer have been published during the past few years (28, 36a, 83, 119). The formal theory for the rate of nonadiabatic electron transfer, k_{et}, generally starts with the following expression:

$$k_{et} = (4\pi^2/h)V^2FC, \qquad 1.$$

where V is the electronic coupling matrix element, and FC is the vibrational overlap (Franck-Condon factor). The electronic coupling matrix element V is proportional to the overlap of the electronic wavefunctions of the donor and acceptor and is the principal origin of the distance dependence of electron transfer. The Franck-Condon factor originates from the requirement that the nuclear configuration of reactants must evolve by thermal fluctuations or vibrations so that the energy of the reactants and products are equal at the transition state between reactants and products. Thus, the FC factor describes the dependence of the rate on the free energy change for electron transfer, ΔG_{et}, and the reorganization energy. The latter accounts for changes in bond length and solvent organization accompanying electron transfer. Although the separation of electronic and nuclear degrees of freedom described in Equation 1 is an approximation and may prove to be oversimplified (S. Franzen & S. G. Boxer, submitted; 119), to date all analyses of electron transfer in proteins have started with this useful formulation.

The rate of electron transfer is expected to fall off rapidly with the distance between the donor and acceptor. In a crude approximation, the overlap of the wavefunction on the donor and acceptor determines this distance dependence: At a considerable distance from each redox active site, the wavefunction falls off roughly exponentially, so one expects an exponential dependence of the rate on the distance. Researchers have estimated the rate of fall-off both theoretically and experimentally for

several systems; the rate decreases by an order of magnitude for each 1.5- to 2.0-Å increase in distance (all other factors being equal) (28, 83). Since the molecules are not necessarily spherically symmetric, there may be an orientation dependence (23). Although determining the overlap of wavefunctions is a standard part of all quantum chemical calculations, the small overlap in long-distance electron transfer presents a problem. The optimization of wavefunctions for quantum chemical purposes primarily depends on the core part of the wavefunction near the nuclei, so the magnitude of the wavefunction tails, for example 10 Å from the nuclear framework, has not been accurately assessed. Furthermore, because matter separates the donor and acceptor (protein, solvent, connecting bridge, etc), the nature of the intervening medium probably perturbs the tails of the wavefunctions, thereby modulating the overlap and rate. This perturbation offers a role for states of the protein or intervening chromophores, discussed later in detail.

The *FC* factors can be estimated using approximate models at various levels of sophistication. The simplest physical picture and that most widely used to analyze data was introduced by Marcus (82, 82a) with

$$k_{et} = (4\pi^2/h)V^2 \cdot [1/(4\pi\lambda kT)^{1/2}] \exp[-(\lambda + \Delta G_{et})^2/4\lambda kT], \qquad 2.$$

where λ is a single parameter characterizing the reorganization energy. The origin of the form of the *FC* factor is easily seen by an analysis of simplified potential energy diagrams describing the reactant and product surfaces (Figure 1). These figures illustrate the normal, optimally exothermic, and inverted regions. As the driving force ($-\Delta G_{et}$) for an electron transfer reaction increases, the vertical displacement of the surfaces increases, so that the rate increases and the activation energy decreases. When $\lambda = -\Delta G_{et}$, k_{et} reaches a maximum value and is activationless. Further increase in the driving force leads to a decrease in the reaction rate and an increase in the activation energy (the inverted region). Note that these plots of *FC* give only relative rates and rationalize the competing effects of ΔG_{et} and λ; to obtain the absolute rate, *FC* must be multiplied by the value of $(4\pi^2/h)V^2$.

More sophisticated treatments of the *FC* factors originate in the theory of radiationless transitions. To include high-frequency vibrational modes, one can use a multiphonon linear coupling model for calculating the Franck-Condon factors (assuming no frequency shifts) (42a, 62a):

$$k_{et} = (4\pi^2/h)V^2 \int_{-\infty}^{\infty} dt \exp[f(t)]; \qquad 3.$$

$$f(t) = \sum_{j=1}^{m} S_i(v_j+1)\exp(ih\omega_j t) + S_j v_j \exp(-ih\omega_j t) - S_j(2v_j+1) - i\Delta G_{et}t. \qquad 4.$$

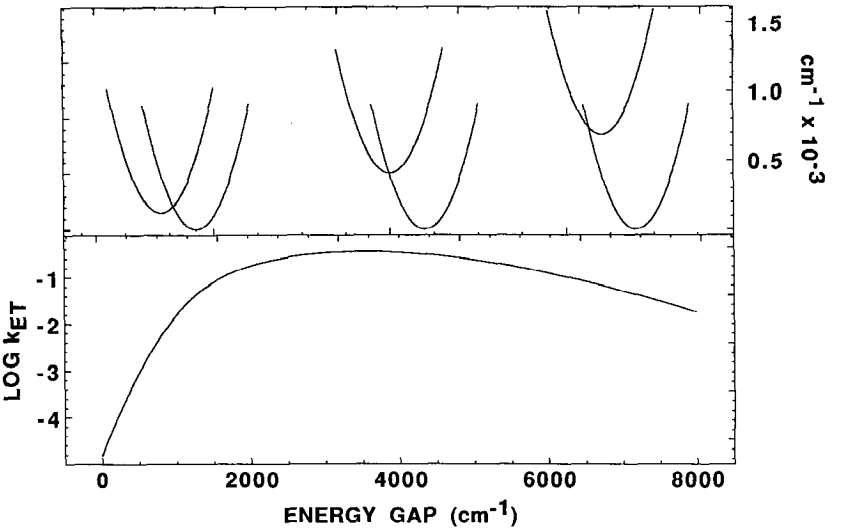

Figure 1 *Upper panel*: schematic reactant and product potential surfaces for electron transfer illustrating the normal, activated region (*left*), the activationless region (*center*), and the inverted, activated region (*right*). *Lower panel*: plot of the logarithm of the rate constant for electron transfer as a function of the driving force or free energy change. This plot was calculated using the saddle point approximation and two modes with linear coupling. The coupling constants are $S_1 = 2.0$ and $S_2 = 40.0$, with corresponding frequencies $\omega_1 = 1000.0$ cm^{-1} and $\omega_2 = 50.0$ cm^{-1} (see Equation 6).

Equation 4 is derived from Equation 1 using the correlation function approach to obtain the Franck-Condon factors (42a). S_j is the nuclear coupling parameter of mode j, and ω_j is the frequency of that mode. The thermal population of the mode is given by v_j:

$$v_j = [\exp(h\omega_j/kT) - 1]^{-1}. \quad 5.$$

Equation 2 is a special case of Equation 4 when $kT \gg h\omega$ for all modes. In Equation 2 the reorganization energy λ equals the sum of couplings and frequencies in Equation 4: $\lambda = \sum S_j h\omega_j$.

The calculation of Franck-Condon factors with linear coupling can be accomplished by several methods. The correlation function (Equation 3) can be expanded using a modified Bessel function that Levich & Dogonadze (70a) proposed first and Jortner (62a) later adapted to biological systems:

$$k_{et} = (8\pi^3 V^2/h^2\omega_s)\exp[-S_s(2v_s+1) - S(2v+1)] \sum_{m=0}^{\infty} [(v+1)/v]^{p(m)/2} \times I_{p(m)}\{2S_s[v_s(v_s+1)]^{1/2}\}[(v+1)/v]^{m/2} I_m\{2S[v(v+1)]^{1/2}\}, \quad 6.$$

where I_m is the modified Bessel function of order m. The k_{et} vs ΔG_{et} curve is then a series of delta functions describing energies that allow electron transfer. In condensed media, some damping occurs owing to the spectrum of phonon frequencies (density of states) in the solvent, which gives width to the delta function transition probability. One common calculational approach uses the modified Bessel function of noninteger order for the low-frequency modes as proposed by Jortner (62a). This approach assumes that the lowest frequency mode (ω_s) determines the density of states. The modified Bessel function approach can be used to calculate the coupling of an electron transfer reaction to an arbitrary number of modes. The form given in Equation 6 is a two-mode function using these assumptions where s is the low-frequency mode. Equation 4 predicts that there will be vibronic structure due to quantum interference effects in the rate as a function of free energy whenever $h\omega \gg kT$. Such structure is not expected in reality because several modes are likely coupled to electron transfer and lead to interference, and the dispersion and damping of low-frequency modes probably minimizes structure. Sarai (111a) presents a variation on the modified Bessel function approach that is easier to calculate. The integral in Equation 3 can also be estimated using the saddle point approximation (42a).

Analyses of experimental data often use Equation 6 with only two modes, or even simpler models with only a single mode, because this makes computation relatively simple, but such analyses can lead to oversimplified conclusions. An important paper on the temperature dependence of the kinetics of the initial charge transfer step in RCs serves as a relevant example (43a). Because the researchers found fitting the data to an unrealistically simple model difficult, an analyst for *Nature* (5) announced: "Electron transfer theory [is] in question"! Experimental variables that affect electron transfer rates, especially in proteins, are often not well enough understood to justify very rigorous comparisons with theoretical expressions, let alone to challenge the theory itself. For example, temperature probably affects the electronic coupling, the free energy, and the reorganization energy, and several modes may be coupled to the initial electron transfer step.

PROPERTIES OF THE REACTION CENTER

The RC is the smallest isolatable unit that performs the initial charge separation steps of photosynthesis (42). The best studied RCs are those isolated from two species of purple bacteria, *Rhodobacter sphaeroides* and *Rhodopseudomonas viridis*. Figure 2 shows the arrangement of the reactive components of the RC from *Rps. viridis* (34); the arrangement of the

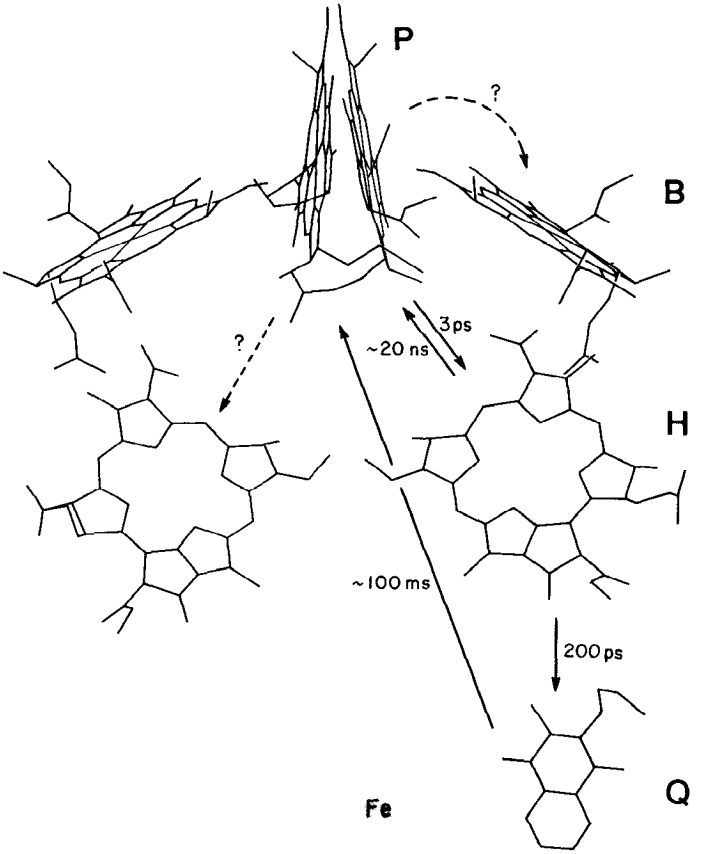

Figure 2 Arrangement of the chromophores in the reaction center of *Rps. viridis* (34). *P* is the special pair electron donor; *B* is the monomeric bacteriochlorophyll *b* on the L-side (right side as drawn) of the RC; *H* is the monomeric bacteriopheophytin *a* on the L-side; *Q* is the quinone (Q_A). The distances among these components are listed in Table 1. The *solid arrows* show the room temperature rates of electron transfer; *dashed arrows* show the reaction pathways that would be expected based on the structure but for which there is little evidence. The approximate C_2 axis of symmetry runs roughly vertically from the geometric center of P to the Fe atom.

chromophores in *Rb. sphaeroides* is similar (1, 2, 24). The chromophores shown in Figure 2 are encased in two hydrophobic proteins, designated L and M, whose combined molecular weight is approximately 60 kd. As isolated, both species of RC contain a third polypeptide that is not associated with the chromophores and in *Rb. sphaeroides* RCs can be removed without affecting function (42). The chromophores in *Rb. sphaeroides* RCs are a-type bacteriochlorophylls (BChl); they are b-type in *Rps. viridis*. The

primary electron donor in both species is a pair of bacteriochlorophylls, often called the special pair, and designated P. Both quinones are ubiquinone in *Rb. sphaeroides*; Q_A is menaquinone in *Rps. viridis*. Both species contain a cytochrome that donates an electron to re-reduce P^+. In *Rb. sphaeroides* the cytochrome is loosely bound and does not cocrystallize with the RC. The cytochrome in *Rps. viridis* is firmly bound, and its structure is also now known (not included in Figure 2) (34). All RCs have a nonheme iron of uncertain function located between the quinones (33). The distances between the components in *Rps. viridis* are given in Table 1.

A remarkable feature of the RC structure is the presence of an approximate C_2 axis of local symmetry roughly along the line connecting the geometric center of dimeric P and the iron atom. Rotation about this axis by 180° exchanges the positions of the two BChls comprising P, the two monomeric BChls(often designated B), the monomeric bacteriopheophytins (often labeled H, BPheo is a BChl in which two protons replace the central Mg ion), and the quinones. The chromophores on the right side of the RC as drawn in Figure 2 are called the L-side chromophores, P_L, B_L, and H_L (the quinone is called Q_A for historical reasons), while the chromophores on the left side are called the M-side chromophores, P_M, B_M, and H_M (the quinone is called Q_B). The designations L and M correspond to the protein subunit that comprises the dominant fraction of the binding site of the chromophore. This labeling misleads because both subunits contribute to most prosthetic group binding sites. The symmetry at the level of the reactive chromophores extends even to the transmembrane α-helices comprising the principle secondary structure of the proteins (35).

Table 1 Distances in Å among chromophores in the *Rps. viridis* RC structure[a,b]

	P_L	B_L	H_L	Q_A	Fe	P_M	B_M	H_M
P_L	—	5.5	9.5	22.4	23.7	2.5	5.7	12.2
B_L	10.4	—	4.8	19.5	25.2	5.4	14.5	17.8
H_L	16.5	10.2	—	9.7	15.5	11.7	18.1	16.9
Q_A	28.2	23.4	14.3	—	6.8	22.8	28.2	19.8
Fe	27.8	26.1	18.0	8.6	—	23.6	26.6	16.2
P_M	7.0	12.6	19.0	28.6	27.8	—	6.1	9.8
B_M	13.0	21.4	24.3	30.9	26.9	10.9	—	5.7
H_M	19.7	24.4	23.4	24.1	18.7	17.1	10.9	—

[a] The values above the diagonal are edge-to-edge distances and those below the diagonal are center-to-center distances.

[b] From (20a). The reader accustomed to small molecule structural data is cautioned that the *Rps. viridis* X-ray structure is at 2.3-Å resolution with an *R*-factor of 0.23, thus typical uncertainties in distance are 0.2 Å or more. Theoretical calculations or interpretations of experimental results sensitive to distance changes of several tenths of an Å are probably not definitive.

The symmetry is broken by slight differences in the distances among the chromophores along the L- and M-branches (Table 1), differences in the orientations of some chromophore ring substituents, and differences in the amino acid side chains on the two proteins. Electron transfer appears to occur almost exclusively along the L-branch, thus also disrupting the symmetry at the level of function. Several investigators (65, 96) have discussed the evidence for this unidirectionality of electron flow in detail, and understanding its origin at the molecular level has become a major challenge for theorists and experimentalists.

ELECTRON TRANSFER REACTIONS IN THE REACTION CENTER

Summary of Reactions To Be Considered

Figure 3 (cf. Figure 2) illustrates in detail the kinetics for the initial forward and recombination reactions in the RC, not including reactions involving Q_B and the cytochromes. Kirmaier & Holten (65) have presented an excellent review. There have been three phases of activity in this area. Prior to the mid-1970s, the kinetics of all reactions with rate constants slower than approximately $10^8\ s^{-1}$ were measured, and the correspondence with the kinetics of paramagnetic species measured by EPR spectroscopy allowed

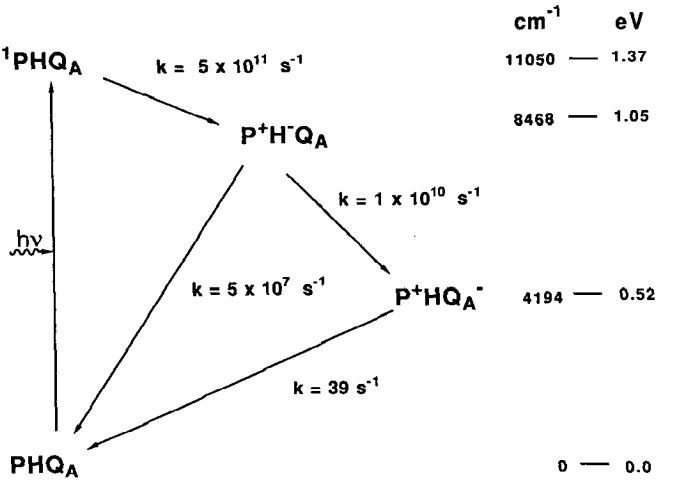

Figure 3 Schematic reaction scheme for the electron transfer steps that have been characterized for *Rb. sphaeroides* reaction centers. The rates are approximately those at 77 K (65). The reverse recombination rates are measured when the subsequent electron acceptor is removed. The energetics of intermediate states are given on the right.

the identification of intermediates (42). The second phase occurred in the mid-1970s with the advent of lasers capable of generating pulses on the order of 10 ps. These lasers permitted measurements of the kinetics of the early steps (63, 111). The intermediates were identified by comparison with the spectra of radical ions of the relevant chromophores, largely the work of Fajer et al (40). The third phase began during the mid-1980s and continues. Lasers with pulse widths as short as tens of femtoseconds have made possible accurate measurements of the kinetics (19, 20, 61, 65, 66, 85, 114, 115, 124) and temperature dependence (43a, 124) of the initial charge separation step in wild-type and mutant (21, 64, 67) RCs.

The initial charge separation step occurs within a few picoseconds from the excited singlet state of the special pair P. The nature of the initial electron acceptor has been a matter of great debate. Examination of the crystal structure (Figure 2) and the fact that the rate of electron transfer falls off rapidly with distance suggest the initial intermediate should be $P^+B_L^-$. Some investigators argue that a measurable concentration of this intermediate does not accumulate during the time of formation of $P^+H_L^-$ (19, 66, 96); Shuvalov and coworkers (114, 115) and recently Holzapfel et al (61) argue that $P^+B_L^-$ formation precedes $P^+H_L^-$ formation. The initial reaction rate increases by a factor of two as the temperature is lowered from room temperature to 5 K (43a). This increase suggests that the reaction is approximately activationless; consequently, within the framework of Figure 1 and Equation 2, the reaction is approximately in the optimally exothermic region of the rate vs free energy profile, and the reorganization energy is approximately equal to the free energy change, estimated to be between 0.17 (125) and 0.26 eV (27, 50). Even with optimized Franck-Condon factors, the electronic coupling would not likely be so large between the reactant ^1PH_L and product $P^+H_L^-$, given the separation of P and H_L, that the rate could approach $10^{12}\ s^{-1}$. Consequently, B_L or intervening amino acid residues must play some role in the reaction, as discussed in detail below.

The next electron transfer step, $P^+H_L^- \rightarrow P^+H_LQ_A^-$, occurs in approximately 200 ps (65). This reaction also speeds up by a factor of two as the temperature is lowered (65). A complicated set of reactions competes with this step. The charges on $P^+H_L^-$ can recombine by reverse electron transfer to reform the ground state PH_L [rate $= 3 \times 10^7\ s^{-1}$ (26)], or they can recombine to form the triplet excited state of P, ^3P [rate $= 4 \times 10^8\ s^{-1}$ (49)], or they can recombine to form the singlet excited state of P, leading to a small amount of delayed fluorescence (125). Any decription of the kinetics of the $P^+H_L^-$ state, therefore, depends on the rates of these competing reactions, and because of the spin multiplicity requirements, the coherent spin dynamics of the $P^+H_L^-$ radical pair must also be properly

considered. This becomes a very complex problem. Only when the $P^+H_L^- \rightarrow P^+Q_A^-$ rate is considerably faster than $10^9\ s^{-1}$ can we consider this step an elementary reaction (48), a fact that has been widely misunderstood. These reactions and their manipulation with magnetic fields are not considered further here but are reviewed elsewhere (12, 14, 58).

When Q_B and cytochrome (Cyt), are not present, so that the reactions $Q_A^-Q_B \rightarrow Q_AQ_B^-$ and $Cyt(II)P^+ \rightarrow Cyt(III)P$, respectively, do not occur, then $P^+Q_A^-$ simply recombines to form the ground state (42). The spin multiplicity of $P^+Q_A^-$ appears not to be important at any temperature likely because the spin on Q_A^- is rapidly relaxed by the paramagnetic nonheme Fe(II). The $P^+Q_A^-$ recombination electron transfer occurs in approximately 100 ms at room temperature and speeds up by a factor of three as the temperature is lowered. Thus, this reaction, which has a driving force of approximately 0.52 eV (3, 125a), also appears to be optimally exothermic. The difference in rates for $^1PH_L \rightarrow P^+H_L^-$ and $P^+Q_A^- \rightarrow PQ_A$ of about ten orders of magnitude, where both reactions apparently are optimally exothermic, largely reflects the difference in distance (see Table 1). Studies of these reactions in electric fields, however, reveal that more subtle features are involved in each reaction.

Although I have presented the information in the previous paragraphs as fact, several uncertainties are worth mentioning. Studying the effect of temperature on reaction rate constants is the traditional approach to obtaining activation energies. Of course, for the study to be useful, the temperature must exclusively affect the electron transfer step. Since the RC is a solid state system at all temperatures at which it is stable (below $\sim$40°C), temperature could affect the distances among the reactants. For example, myoglobin has been shown to contract as the temperature is lowered. The contraction is not uniform, however. On average, two points decrease in distance by 3–5% as the temperature of a crystal is lowered from room temperature to cryogenic temperatures (45). The RC structure has not yet been delineated at low temperature, but if the myoglobin result proves typical, it can have significant consequences for the interpretation of rates as a function of temperature in the RC. For example, P and Q_A are separated by approximately 25 Å. If this distance decreased by 5% (1.25 Å) as the temperature is lowered, one would predict that the $P^+Q_A^-$ recombination rate could speed up by nearly one order of magnitude due to the shrinkage alone. Likewise, the increase in the rate of the initial reaction as the temperature is lowered could be largely due to a distance change of 0.5 Å or a change in the orientation of a side chain [this possibility was ruled out in (43a) for no apparent reason]. Also, as the temperature changes, the participation of different activated pathways may become important. In particular, whenever the participation of virtual

states of the medium (amino acids, other chromophores, etc) is invoked in a superexchange mechanism, a parallel activated pathway exists. This change in pathway can greatly complicate the analysis of electron transfer reactions. Finally, in the context of Figure 1 and Equation 2, a common assertion is that when an electron transfer rate exhibits little dependence on temperature, $\lambda = -\Delta G_{et}$. If more sophisticated models are used, however, then reactions may show a much reduced temperature dependence as a function of ΔG_{et} (54).

The experimental perturbations readily available for probing electron transfer reactions in the RC include temperature, pressure, isotopic composition, quinone substitution, pH, ionic strength, magnetic and electric fields, and genetic manipulation. Each type of perturbation has some shortcomings, generally because more than one factor changes. The effects and complications of temperature have been discussed. Few studies have focused upon pressure; hydrostatic pressure alters many degrees of freedom in the RC, and these phenomena are difficult to evaluate separately (60, 121). Perdeuteration was not observed to affect the kinetics of the initial charge separation step (43a); however, a small increase of the $P^+Q_A^-$ recombination rate was observed when RC protons were exchanged for deuterons, and the protons were identified by ENDOR (100). Numerous quinones have been substituted in the Q_A (42, 53, 54, 125a) and Q_B binding sites (46) to measure consequences of variations in the quinone redox potential on the rate of formation or decay of Q^-. This work will be discussed further below. To date no other reactive component of the RC has been substituted. B_M can be removed by treatment with $NaBH_4$ (38) with no detectable effect on the reaction dynamics (65), and genetic manipulation (21, 64, 67) makes possible some systematic changes. For further discussion of genetically modified photosynthetic reaction centers, see Coleman & Youvan's (28a) review in this volume. Magnetic fields affect the lifetime and yield of intermediates and products whose formation or decay involves $P^+H_L^-$ when Q_A is either removed or reduced (3, 12, 14, 58). The effect of electric fields offers a selective approach to the manipulation of electron transfer reactions.

Electric Field Effects on Electron Transfer Reactions

The effect of an electric field on the absorption or emission spectrum of a molecule, also known as the Stark effect, has been used for many years to measure the properties of electronic states (57, 74, 86, 87). The Stark effect spectrum can provide information on changes in the dipole moment $\Delta\mu$ associated with an optical transition, on changes in polarizability $\Delta\alpha$, and on field-induced changes in the oscillator strength. In addition, we can determine the angle between the directions of $\Delta\mu$ and $\Delta\alpha$ and the transition

dipole moment for the absorption or emission feature used to probe the Stark effect; since the direction of the transition dipole moment relative to the molecular axes can be measured by polarized single crystal spectroscopy, the directions of $\Delta\mu$ and $\Delta\alpha$ relative to the molecular axes can be obtained. The direction of $\Delta\mu$ is especially useful in evaluating the RC because it reflects the direction of charge displacement associated with an optical transition.

In practice, Stark effects can be measured either on samples that are oriented or isotropic with respect to the field. The former is preferable so long as the degree of orientation is known accurately (e.g. a single crystal is ideal), but one can obtain a great deal of quantitative information from isotropic samples. In simple terms, the energies of the difference dipoles $\Delta\mu$ increase or decrease depending on their orientations in an external field, and this change leads to a broadening of the absorption or emission band. When $\Delta\mu$ dominates other effects and remains constant across the band, the change in absorption or emission then equals approximately the second derivative of the absorption or emission lineshape. If the change in polarizability dominates, then the absorption or emission lineshape shifts in the field to yield a first-derivative lineshape. A field-induced change in oscillator strength increases or decreases the absorption or emission intensity, resulting in a zeroth derivative change in the lineshape. As will be seen below, the study of emission needs special consideration because the zero-field time constant for emission (e.g. the fluorescence lifetime) is like an internal clock, and electric field–dependent processes may compete with emission. Changes in the emission intensity in an applied electric field can then be used to study the mechanism of competing reactions such as electron transfer.

Electric field effects are a natural subject for study because the RC spans a membrane that can have a substantial transmembrane potential. For an idealized bilayer 50 Å thick, a transmembrane potential of 500 meV (somewhat larger than is likely to be physiologically relevant) corresponds to an applied electric field of 10^6 V/cm (10 meV/Å). Since the RC is oriented with respect to this applied potential, the energies of dipolar states such as $P^+H_L^-$ and $P^+Q_A^-$ change: $\Delta U(F) = -\mu \cdot F$, where F is the applied electric field. For example, the $P^+Q_A^-$ dipole is roughly aligned with the local C_2 axis (see Figure 2), which is parallel to the membrane normal, and $|\mu(P^+Q_A^-)| \approx 130$ D based on the crystal structure (34). Thus, the energy of this dipole increases by nearly 300 meV for a field of 10^6 V/cm, a substantial fraction of the 520 meV ΔG_{et} (3, 125a) for the $P^+Q_A^- \rightarrow PQ_A$ recombination reaction. For the same applied field in a bilayer, the effect on the driving force for the initial charge separation reaction will be smaller because $|\mu(P^+H_L^-)| \approx 80$ D, and the dipole is less parallel to the C_2 axis.

Feher and coworkers (41, 51, 68) have measured electric field effects on the $P^+Q_A^-$ recombination reaction in lipid bilayers, and Popovic et al (107–109) have measured the $P^+Q_A^-$ recombination kinetics and formation quantum yield in Langmuir-Blodgett films. Further results of these experiments will be discussed below.

One can also measure electric field effects on samples in which the RCs are randomly oriented with respect to the applied field. This approach is technically much easier than orienting the sample. RCs in poly(vinyl-alcohol) matrices can be coated with semitransparent Ni electrodes by vapor deposition (75) or can be sandwiched between slides coated with semitransparent electrodes (81). Alternatively, one can study samples frozen in glycerol-water glasses between transparent electrodes (117). A researcher can readily obtain applied electric fields in excess of 10^6 V/cm for PVA films at low temperature, while achieving somewhat lower fields with frozen glasses before dielectric breakdown. The obvious disadvantage of working in isotropic samples is that the energies of dipolar states spread upon application of the field rather than simply shift. Nonetheless, with appropriate analysis of high-quality decay data, one may obtain information on the electron transfer mechanism. Because the interaction between the field and dipoles is intrinsically anisotropic, a researcher can also obtain angle-dependent information that can be analyzed using the crystal structure.

Electric Field Effects on the Initial Charge Separation

Our research group (17, 55, 56, 75, 76) and several others (18, 36, 37, 80, 81) have used Stark effect spectroscopy to probe the properties of the excited state of the primary electron donor, ^1P, in RCs from various species of bacteria and for some mutants. Figure 4 illustrates a key result: the absorption Stark effect for the lowest electronic transition of the special pair is substantially larger than for the monomeric bacteriochlorophylls (B_L and B_M) and bacteriopheophytins (H_L and H_M). The approximately second-derivative lineshape indicates that the change in dipole moment between the ground and excited state dominates the effect. Considerable speculation has centered on the origin of this difference, although no consensus has been reached. The prevailing view, discussed elsewhere in detail (14), is that ^1P is considerably more polar than the ground state because it is mixed with charge transfer states of the special pair itself, sometimes called P^+P^-, and/or with $P^+B_L^-$ (103, 120, 123). [Studies of RCs in which B_M was removed have ruled out mixing with states involving this chromophore (55).] Consistent with this interpretation, the direction of charge displacement lies between that predicted for the P^+P^- and

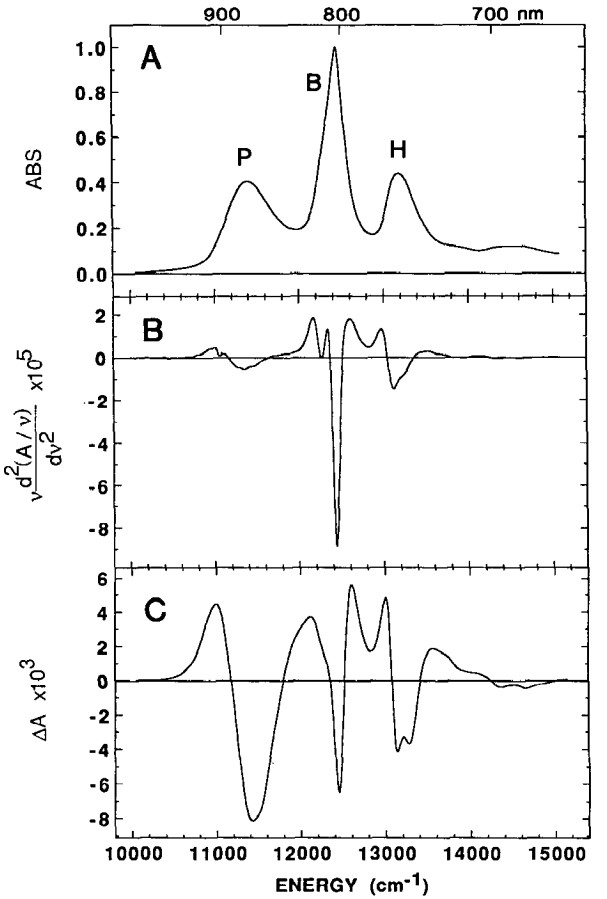

Figure 4 Absorption (*A*), second-derivative (*B*), and Stark effect (*C*) for *Rb. sphaeroides* RCs in a PVA film in the Q_y region at 77 K. The data have been scaled to *A*(802) = 1.0 and $F_{ext} = 1.0 \times 10^6$ V/cm.

$P^+B_L^-$ dipoles (the directions are estimated using the crystal structure) (75). Studies of a mutant of *Rb. sphaeroides* in which the Mg from the M-side bacteriochlorophyll of the special pair has been lost following replacement of its His ligand by Leu, using site-specific mutagenesis, further support this interpretation (22, 112). The so-called heterodimer mutant exhibits a strong feature in the Stark spectrum with a linewidth comparable with that in the wild type, as shown in Figure 5 (37, 56). The magnitude of $|\Delta\mu_A|$ for this feature is about two times greater than that for the homodimer (56). Because bacteriopheophytin is considerably easier to reduce than

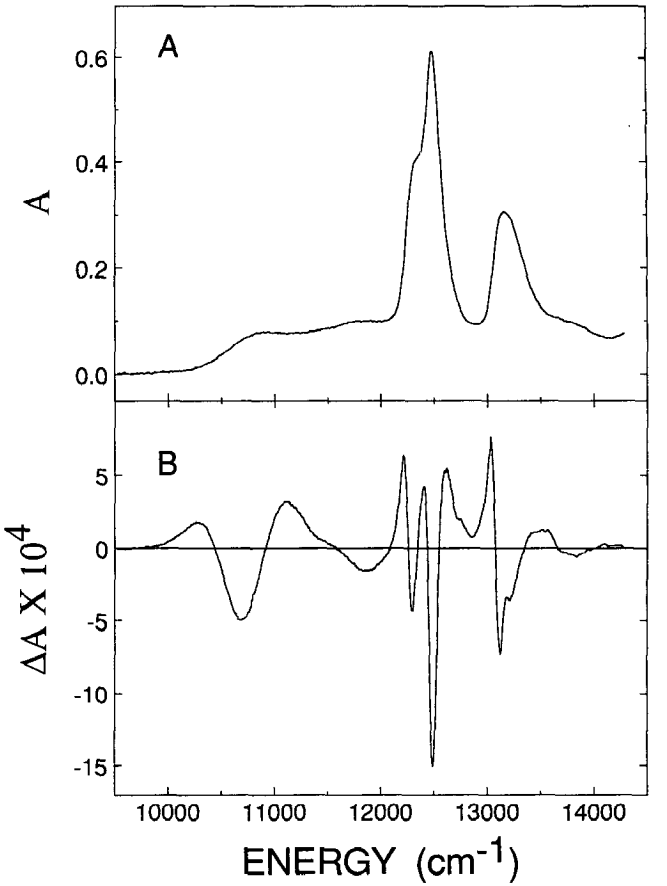

Figure 5 (*A*) Absorption and (*B*) Stark effect spectrum in the Q_y region of the heterodimer mutant M(H200L) of *Rb. sphaeroides* RCs at 77 K in a glycerol-water (50/50: v/v) glass ($F_{ext} = 2.14 \times 10^5$ V/cm, $\chi = 54.7°$). $\Delta\mu_A$ for the lowest energy band is approximately twice as large as for P in wildtype (cf Figure 4) (56).

bacteriochlorophyll (40), charge-transfer states of the heterodimer (e.g. $P_L^+P_M^-$) are expected to be lower in energy than those for the homodimer (40, 64). Thus, the larger magnitude of $\Delta\mu_A$ for the heterodimer's lowest electronic transition and the red-shift of its absorption maximum are consistent with increased mixing of charge-transfer character into the excited state (103, 120) of this dimer. Both for the homo- and heterodimer, these results suggest that charge separation is initiated upon photo-excitation (75).

We have also measured the Stark effect on the fluorescence from the

special pair in several species of bacterial RCs (77) and in photosystem II RCs (117). In all cases, the result strikingly contrasts that obtained for the absorption spectrum. Instead of the characteristic second-derivative lineshape seen in Figures 4 and 5, the fluorescence increases substantially in the field, as shown in Figure 6. The increase in fluorescence is quadratic in the applied field strength (Figure 7) (77, 78). Because little evidence supports a zeroth-derivative contribution to the absorption Stark effect for the special pair, the large zeroth-derivative effect on the emission is probably not due to a change in the intrinsic radiative rate of the dimer. Instead, we have argued that the increased fluorescence in an applied field results from a net slowing in the rate of a competing process, specifically the rate of the initial charge separation step (77). Measurements of the kinetics of the initial charge separation directly in an applied field have confirmed this suggestion (16, 79).

Figure 8 illustrates a simple reaction scheme to make this idea clearer. The quantum yield of fluorescence, Φ_f, is given by

$$\Phi_f = k_f/(k_f+k_{nr}+k_{et}), \qquad 7.$$

where k_f is the radiative rate, k_{nr} accounts for any nonradiative decay

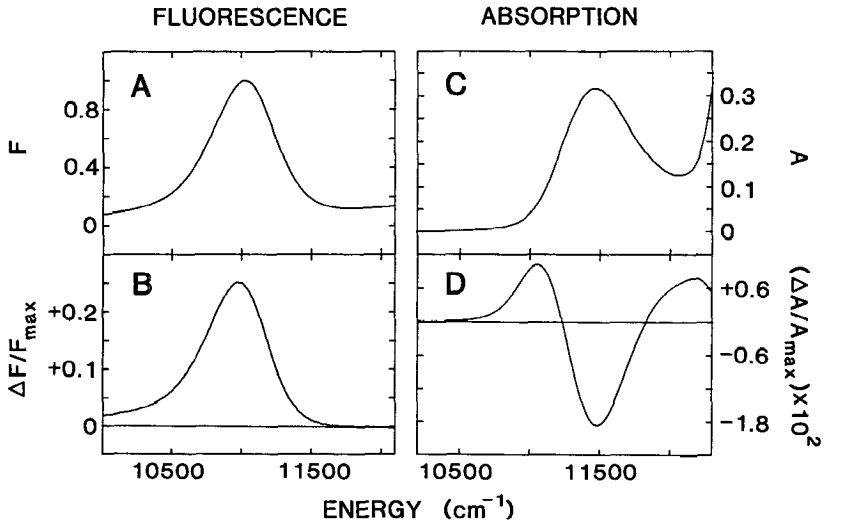

Figure 6 (*A*) The fluorescence spectrum of quinone-depleted *Rb. sphaeroides* RCs in PVA at 77 K in the absence of a field, and (*B*) the change in the fluorescence intensity for the same sample in a field of 8.9×10^5 V/cm. (*C*) The absorption spectrum of the Q_y transition of the special pair in quinone-depleted reaction centers in PVA at 77 K, and (*D*) the change in the absorbance for the same sample in a field of 8.9×10^5 V/cm.

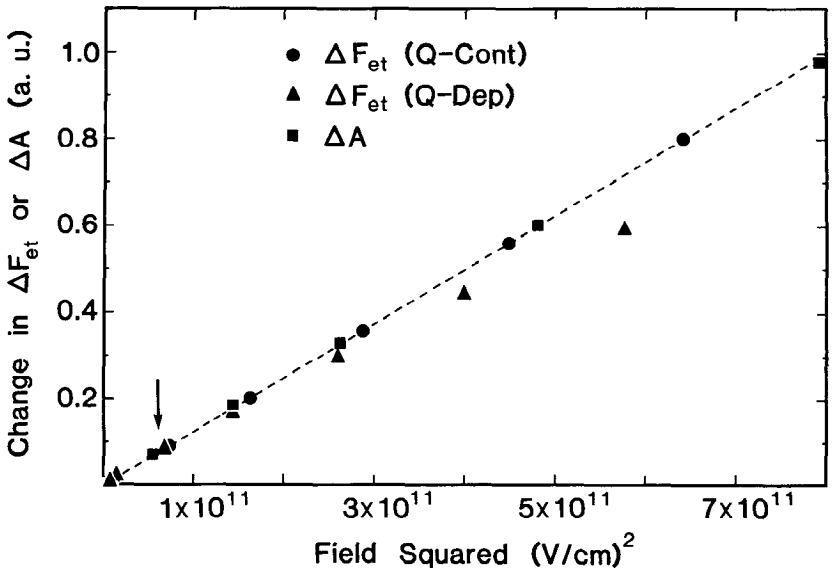

Figure 7 The dependence of the change in absorbance (*squares*) and the fluorescence intensity for quinone-depleted (*triangles*) and quinone-containing (*circles*) RCs on the square of the applied field strength for the Q_y transition of the special pair in *Rb. sphaeroides* RCs in PVA at 77 K. The same dependence of the change in fluorescence for quinone-depleted RCs is observed using a dc and ac applied field. This quadratic-field dependence places significant restraints on the rate vs free energy profile for the initial charge separation reaction (cf Figure 1).

processes, and k_{et} is the rate constant for P^+I^- formation (I is the initial electron acceptor, either B_L or H_L). Assuming that k_{et} is the only rate dependent on electric field, and recognizing that k_{et} is much faster than either k_f or k_{nr} [this recognition is consistent with the known quantum yield of fluorescence (128) and the measured k_{et} (20, 85, 124)], the fluorescence quantum yield is simply inversely proportional to k_{et}. One of the effects of the electric field on k_{et} can be seen by reference to Figure 1: since the initial charge separation reaction is approximately activationless, the rate at zero field is near the top of the k_{et} vs ΔG_{et} curve. As illustrated in Figure 8, in an isotropic sample, the energy of the P^+I^- dipole increases or decreases depending on its orientation in the applied electric field. Since at zero field the system is near the top of the k_{et} vs ΔG_{et} curve, however, the net effect of either an increase or a decrease in ΔG_{et} will be to decrease k_{et} and increase the fluorescence quantum yield. The absolute magnitude of this effect depends explicitly on the shape of the k_{et} vs ΔG_{et} curve in the vicinity of the zero-field ΔG_{et}.

The physical picture developed in the previous paragraph implies that

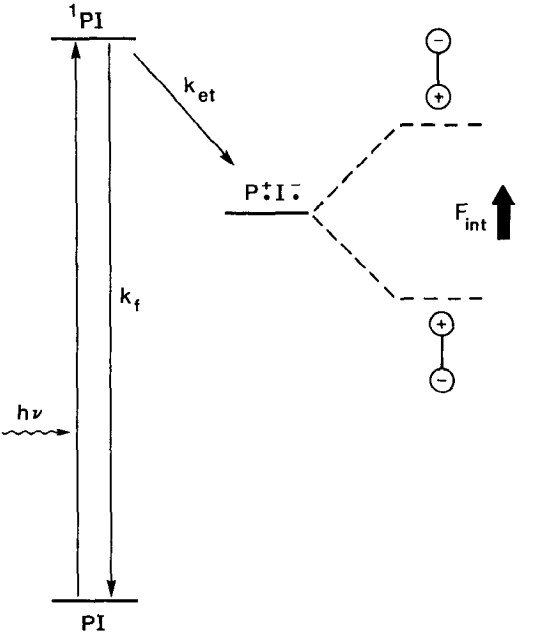

Figure 8 Definition of dipole moments of states and difference dipole moments. The *solid lines* are schematic energy levels in zero electric field. For an isotropic immobilized sample in an applied electric field, the energy of the P^+I^- state increases or decreases depending on the orientation of the P^+I^- dipole; the largest changes occur for dipoles oriented parallel or antiparallel to the field (*dotted levels*). The ground and excited states of P may also have nonzero dipole moments; however, these are assumed to be much smaller than the P^+I^- dipole moment and are not shown for simplicity. The intermediate electron acceptor I may be either B_L or H_L (cf Figure 2) as discussed in the text.

the rate of the initial charge separation reaction should depend on the orientation of the RC in an electric field because the energy of the product state depends on orientation. If k_{et} depends on orientation, then Φ_f also depends on orientation. In other words, the fluorescence should become polarized upon application of an electric field. We have observed this effect and have analyzed it quantitatively (78). The electric field–induced fluorescence anisotropy depends on the angle between the dipole for which energy is being modulated and the transition dipole moment for fluorescence. Until now we have assumed that the relevant dipole is the 80 D $P^+B_L^-$ dipole; however, formation of the 50 D $P^+B_L^-$ dipole may compete with fluorescence if electron transfer to B_L is the initial step. Given a reasonable body of data on the orientation of the transition dipole moment, we can estimate the expected angle, assuming that $P^+B_L^-$ or

$P^+H_L^-$ dipole formation is important, and that the charges on P^+, B_L^-, and H_L^- can be approximated by using the geometric centers of the macrocycles. Better estimates might be obtained by considering the charge densities measured over long times for P^+ and H_L^-, but these estimates may not be more relevant to the early time (picosecond) properties of the initially formed ion pair. Furthermore, the observed angle dependence relies on the difference dipole between the product state and the ^1P state, for which little direct experimental data is available. The experimentally determined angle is inconsistent with the estimated angle if formation of $P^+B_L^-$ competes with fluorescence (78) when one uses the simple model for the dipole direction. Thus, both angle-measurement experiments and much of the transient kinetic data (19, 66) suggest that $P^+B_L^-$ does not accumulate to any appreciable extent during the formation of $P^+H_L^-$. The precise mechanism of this early reaction is still a matter of considerable controversy.

As mentioned at the outset, the physical separation of P and H_L argues strongly that the rate of direct electron transfer from ^1P to H_L without participation of the intervening medium should be much smaller than 10^{12} s^{-1}. Various mechanisms have been proposed to escape from this dilemma; the most popular is a superexchange mechanism in which states of the intervening bacteriochlorophyll B_L mediate (enhance) the interaction between ^1P and H_L without actually populating those states (10, 43, 96, 120). For other electron transfer reactions, aromatic amino acids may play a similar role. The orbitals on B are so much lower in energy than those of aromatic amino acids that the latter are generally not considered in discussions of the initial charge separation step in the RC. Residues in the vicinity of B_L may exert electrostatic control (96). For convenience, we introduce the following notation (see Figure 9): State $1 \equiv {}^1PBH$; State $2 \equiv$ mediating state, e.g. P^+B^-H or P^1BH; State $3 \equiv P^+BH^-$ (only B_L and H_L are considered). In this model, the electronic coupling between the initial and final states of the electron transfer reaction is enhanced by virtue of electronic coupling between the initial and mediating state, V_{12}, and between the mediating and final state, V_{23}. The overall electronic coupling, V_{et}, also depends on the energy difference, ΔE_{12}, between the initial state and the mediating state at the nuclear configuration Q_{13} where the potential energy surfaces of the initial and final state cross (see Figure 9). According to standard treatments (9, 10, 14, 96, 106), one obtains

$$V_{et} = \frac{V_{12}V_{23}}{\Delta E_{12}(Q_{13})}, \qquad 8.$$

where

$$V_{12} = \langle 1|\mathscr{H}_1|2\rangle$$

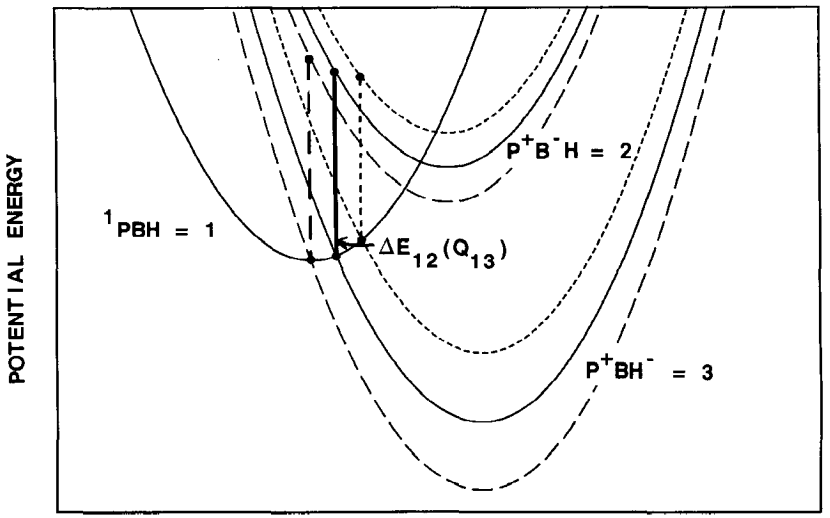

Figure 9 Schematic illustration of the relevant potential energy curves as a function of nuclear configuration for a superexchange mechanism for the initial electron transfer reaction in the RC. State 1 ≡ ^{1}PBH, State 2 ≡ mediating state, e.g. P^+B^-H or P^1BH, State 3 ≡ P^+B^-. (*Solid line*) Zero field curves for the initial, mediating, and final states. Potential energy curves in the presence of an electric field that is aligned (*long-dashed line*) or opposed (*short-dashed line*) to the permanent dipole moment of the final state. The dipole moment of the initial state is asumed to be negligible, and the dipole moment of the mediating state is assumed to be half as large and in the same direction as that of the final state. Q_{13} is the value of Q at which the curves for the initial and final states cross along the relevant reaction coordinate, and $\Delta E_{12}(Q_{13})$ is the vertical energy difference between the curves for states 1 and 2 at this value of Q_{13}. Note that moving the curve for state 3 vertically relative to that for state 1 (a change in ΔG_{et}) changes Q_{13} and thus $\Delta E_{12}(Q_{13})$, even if the curve for state 2 remains fixed (as would be the case if state 2 is relatively nonpolar, e.g. if state 2 is P^1BH). The qualitative features of the figure are expected to apply generally to long-distance electron transfer reaction between neutral molecules. For long-distance electron transfer reactions between two sites separated by molecules in the intervening medium (e.g. aromatic or aliphatic spacers, solvent molecules, amino acids), states involving the medium might participate. In these cases, the mediating state is likely intermediate in overall nuclear configuration between the initial and final state, and the dipole of the mediating state (if it is dipolar) is probably intermediate in magnitude and approximately parallel to that of the final state.

$$V_{23} = \langle 2|\mathscr{H}_1|3\rangle$$

$$\Delta E_{12}(Q_{13}) = E_2(Q_{13}) - E_1(Q_{13}) \gg V_{12}.$$

$\mathscr{H}_1$ is the Hamiltonian of the interaction that couples the states, and $\Delta E_{12}(Q_{13})$ is the energy difference between the initial state and the mediating state at the nuclear configuration of the intersection of the electron

transfer initial and final state potential surfaces, Q_{13} (not the energy difference between the states at their individual equilibrium nuclear configurations).

In addition to the field effect on *FC* (through a change in the energy of P^+H^- leading to a change in ΔG_{et}, cf Figure 1), an electric field can also affect V_{et} by changing ΔE_{12} in two ways: (*a*) the energy of the mediating state is changed by the field (this is especially important if the mediating state is very dipolar); (*b*) a change in ΔG_{et} also results in a change in Q_{13} (97). Since the initial and mediating state potential energy surfaces are not flat, $\Delta E_{12}(Q_{13})$ changes because the value of Q_{13} changes. As a result, ΔE_{12} can be field dependent owing to a dipolar final state, even if the mediating state is nonpolar. Specifically, assuming that the potential energy curves for the initial, mediating, and final states are harmonic and that they have the same shape, in an electric field F (see Figure 9), the result is

$$\Delta E_{12}(F) = \Delta E_{12}(F=0) - \mu(2)\cdot F + (\lambda_{12}/\lambda_{13})^{1/2}[\mu(3)\cdot F], \qquad 9.$$

where λ_{ij} is the reorganization energy (79).

Other reports (9, 14, 79) give a much more detailed analysis of the electric field effects in the context of a superexchange mechanism. As shown in Figures 6 and 7, for a field of 10^6 V/cm, the fluorescence intensity increases by about 40%, and the change in fluorescence is quadratic in field up to 10^6 V/cm. If the form of the Franck-Condon term is similar to that given by Marcus theory (Equation 2) or any related form that has a very steep dependence of k_{et} on ΔG_{et}, it can be shown that this term dominates the field effect on the rate at high field and the dependence is predicted to be superquadratic (9, 79). The effect of the field on the electronic coupling will either enhance or mitigate this dependence. Because the $P^+B_L^-$ and $P^+H_L^-$ dipole directions are of comparable magnitude and direction (obviously not identical), we expect the potential surfaces describing these states to shift approximately in parallel for different orientations of RCs in the field. We currently believe that all the data require that the dependence of the rate on free energy for the initial charge separation step is much less steep than that predicted by the Marcus theory, suggesting substantial coupling to at least several modes. The magnitude and field dependence of the fluorescence also place severe constraints on a mechanism that involved initial formation of $P^+B_L^-$ as a discrete intermediate (79).

Electric Field Effects on $P^+Q_A^-$ *Recombination*

Previous measurements of electric field effects on the $P^+Q_A^-$ recombination reaction in oriented systems, bilayers (41, 51, 69), and Langmuir-Blodgett films (107, 109) at room temperature gave very different results. We have

explored this further by measuring the decay kinetics in nonoriented systems, partly to resolve this discrepancy and partly to develop the general experimental and analytical methodology (44). If the electron transfer kinetics at zero-applied field can be accurately characterized by a single exponential, then the application of a field will increase and decrease ΔG_{et} depending on the orientation and magnitude of dipolar states, leading to a distribution of decay rates. In general, the mapping of ΔG_{et} onto k_{et} is very nonlinear, as illustrated in Figure 1; consequently the kinetics for an isotropic sample become highly nonexponential in an electric field. Nonetheless, we have shown in model calculations that the deviation from exponentiality upon application of the field is characteristic of the shape of the k_{et} vs ΔG_{et} curve in the vicinity of the zero field ΔG_{et} (13, 15). By measuring the decay kinetics very accurately as a function of field strength, we can produce a family of electromodulated decay curves and determine a continuous experimental k_{et} vs ΔG_{et} curve.

To date we have investigated the low-temperature (20–80 K) $P^+Q_A^-$ decay kinetics in greatest detail. The decay at low temperature is not complicated by competing activated recombination pathways; however, many studies (27a, 68, 102, 113) have noted that the decay is bi-exponential at low temperature. The origin of these two decay components is not well understood but probably reflects varying degrees of protonation. Figure 10 shows examples of the effects of the field on the decay kinetics, and Figure 11 displays the experimental k_{et} vs ΔG_{et} curves obtained from a quantitative analysis for the two decay components (44). The k_{et} vs ΔG_{et} curves are relatively flat compared with the prediction of the semiclassic Marcus theory (Equation 2). The curves are markedly asymmetric and are much flatter for larger values of $-\Delta G_{et}$ than for smaller values. This lineshape argues that many modes, including both low- and high-frequency modes, are coupled to the electron transfer process (cf Figure 1*B*). The maximum rate is not the zero-field rate, so even though the reaction is essentially activationless, the reorganization does not equal the zero-field free energy, although it comes close. The curves give no evidence of structure. The experimental curves are continuous because a continuous distribution of ΔG_{et} is sampled between $\pm\mu(P^+Q_A^-)F$ [at the highest applied fields this distribution covers a range in excess of ± 300 meV since $\mu(P^+Q_A^-) \approx 130$ D], in contrast to data obtained with model compounds at discrete points (28). Finally, the shape of the curves for the two decay processes is quite different, reflecting some (as yet unexplained) differences in the modes that are coupled to the electron transfer process.

Because the data presented earlier for oriented systems was measured at room temperature, we cannot directly compare these methods. Gunner et al (54) have provided some evidence that the k_{et} vs ΔG_{et} curve for this

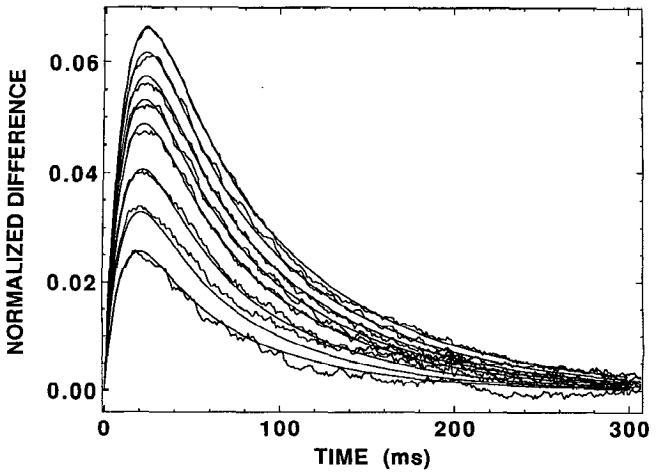

Figure 10 Difference decay curves (field-on minus field-off) for $P^+Q_A^-$ charge recombination at 80 K for an isotropic sample of *Rb. sphaeroides* reaction centers. Data are shown for external fields 7.61, 8.57, 9.05, 9.52, 10.00, 10.47, 10.96, and 11.43 $\times$ 10^5 V/cm where increasing fields lead to larger differences relative to zero field (44). This directly demonstrates an electric field effect on the rate of electron transfer and can be used to extract the rate vs free energy curve for this reaction. The lines through the data were generated from the parameters obtained from the best fit to the data using a cumulant expansion in powers of the field (see Figure 11).

reaction is not strongly temperature dependent. If so, one could compare data at different temperatures. The data in Figure 11 is quite similar to that obtained by Feher and co-workers using bilayer samples (41, 51, 68). It differs a lot from data obtained in Langmuir-Blodgett films (107, 109). Gunner et al (54) have measured $P^+Q_A^-$ recombination for RCs in which the native Q_A (ubiquinone) has been substituted with numerous other quinones over a considerable range of ΔG_{et}. The recombination kinetics were measured by EPR spectroscopy at low temperature. The EPR decay curves were explicitly treated as single exponential curves, however, making any direct comparison of results with those in Figure 11 difficult. Although calculated curves similar to the experimental k_{et} vs ΔG_{et} curve shown in Figure 11 were drawn through the quinone-substituted decay data (54), the experimental scatter was large enough to obscure the meaningfulness of the agreement with the experimental curves in Figure 11. Nonetheless, the emerging picture shows that both low- and high-frequency modes may play significant roles in determining the electron transfer rate in this slow long-distance recombination reaction, similar to the view suggested earlier for the very fast initial reaction (79).

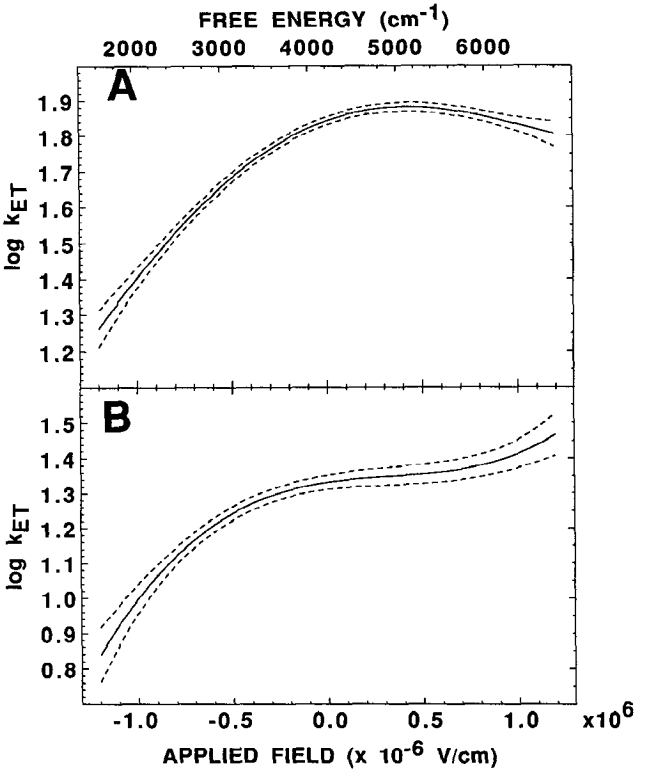

Figure 11 Experimental log k_{et} vs ΔG°_{et} curves for $P^{+}Q^{-}_{\bar{A}}$ charge recombination obtained from the best fit to the electromodulated kinetic data shown in Figure 10. The *dotted curves* above and below the best fit represent the errors in the curves. (All curves are continuous because the electric field modulation for an isotropic sample samples a continuous distribution of free energies). The $P^{+}Q^{-}_{\bar{A}}$ decay kinetics are biphasic at 80 K. Panels *A* and *B* are log k_{et} vs G°_{et} curves obtained for the fast and slow components, respectively (44).

ELECTRON TRANSFER IN OTHER PROTEINS

General Comparisons

Many studies have examined bimolecular electron transfer between proteins and various redox reagents or other redox proteins. The importance of diffusion and targeting of the redox centers in such systems makes comparison of such bimolecular examples with the RC difficult, and these will not be considered further. During the past few years, many studies have reported on electron transfer within tight complexes of proteins, presumably unimolecular reactions, and researchers have covalently modified several proteins with redox active groups to examine the factors that

influence electron transfer rates. In nearly all of these examples, one or both redox centers is a transition metal, e.g. Fe(II)/Fe(III) in heme or an iron-sulfur center, or Ru(II)/Ru(III) covalently linked on the protein surface. Rather substantial bond-length changes accompany changes in the oxidation states of many inorganic complexes (83). By contrast, the changes in bond length for oxidation or reduction of a porphyrin or chlorin to form π-cations or anions involves only a single electron out of many π-electrons. Consequently, only small structural changes occur. Furthermore, the charge is spread out in macrocyclic π-cations and anions, whereas it is much more localized in inorganic redox centers. For these reasons, the inner sphere reorganization energy is likely greater for electron transfer involving transition metal ion centers than for large organic chromophores (e.g. chlorophylls). Similar arguments concern quinones: formation of the semiquinone anion radical leads to a substantial change in the carbonyl bond length and the negative charge is relatively localized. Water molecules often play a central role in transition metal complex redox chemistry either because the redox center is on the protein surface and exposed to bulk water or because water molecules are associated with a buried redox center, such as for ferric heme in the metaquo form. If the movement of water molecules is closely coupled to electron transfer, a large, outer-sphere reorganization energy is expected. By contrast, the initial charge separation step in RCs takes place in the very hydrophobic environment of the membrane interior. The initial step is essentially activationless and, therefore, ΔG_{et} [at most 0.26 eV (27, 50, 125)] approximately equals the reorganization energy. Most of this small total reorganization energy is probably associated with small changes in the bond lengths that occur when P becomes P^+ and H_L becomes H_L^-. Comparisons between electron transfer in the RC and in other systems must therefore be made for comparable separations and for a comparable balance between the reorganization energy and ΔG_{et}—not always an easy task.

Modified Proteins in Physiological Complexes

The basic questions described at the outset of this review have been addressed by studies of model protein systems. Now we will discuss two classes of proteins modified to examine electron transfer properties: complexes between physiological partners and proteins modified on the surface with redox active groups. The first class includes mixed-metal hemoglobins in which either the α- or β-chain is substituted with a porphyrin whose triplet lifetime and energetics (e.g. Zn-protoporphyrin IX) are sufficient to photoreduce a ferric heme in the other chain (47, 89, 90, 104, 105). This complex remains stable as the physiological $\alpha_1\beta_1\alpha_2\beta_2$ tetramer under appropriate conditions. The distance between the metal centers is approxi-

mately 25 Å, comparable with the $P^+Q_A^-$ separation: The driving force is approximately 0.8 V, compared with about 0.52 V for $P^+Q_A^-$ recombination. Unlike in the RC, the electron transfer reaction takes place across a hydrophyllic subunit interface. At room temperature, the rate of electron transfer, $^3ZnP \rightarrow Fe(III)$ is about 100 s^{-1}, which compares well with the rate for $P^+Q_A^-$ recombination. The rate of electron transfer in the hybrid hemoglobins decreased by a factor of 2–3 as the temperature was lowered, with no further decrease below approximately 200 K (90). This temperature dependence markedly contrasts with the $P^+Q_A^-$ recombination, which speeds up as the temperature is lowered. The difference presumably results from a significant difference in the reorganization energy.

Several years ago our group prepared complexes in which chlorophyll derivatives were substituted in either the α- or β-chains and heme was left in the other chains (70, 98). These systems were designed for studies of singlet energy transfer between partners at a fixed distance and orientation. Because the chlorin triplet lifetime is about two orders of magnitude shorter than Zn-protoporphyrin IX, we did not detect electron transfer. However, the singlet lifetime of chlorophyll depends on the state of the heme 25 Å away. This dependence results from differences in the rates of irreversible energy transfer (chlorophyll → heme followed by radiationless decay) due to small differences in very weak absorption features in the heme. This example serves to illustrate one of the dangers in some model studies of electron transfer. Although transient absorption spectra can suggest that electron transfer, rather than energy transfer, occurs, the experimenter should confirm electron transfer by a method explicitly sensitive to charge or spin changes (e.g. EPR kinetics) and determine corresponding kinetics for spectral changes on both the donor and acceptor. McGourty et al (90) have taken great care to assure that electron transfer is actually measured in the modified hemoglobin complexes.

Studies of complexes between cytochrome *c* peroxidase or cytochrome b_5 and cytochrome *c* examined a second group of systems based on physiological redox partners (25, 29, 30, 56a, 71, 72, 91–93, 116). A structural model for the cytochrome peroxidase-cytochrome *c* complex was suggested several years ago (110). Multiple conformations are likely present in solution (no crystal structure of the complex has been determined yet). When the rate of conformational changes or changes in subunit interactions becomes rate limiting, then the observed rate of electron transfer actually measures the time scale for conformational transitions. This situation has been named *conformationally gated electron transfer* (59), an expression that is somewhat confusing because *conformational gating* is often used to describe conformational changes in response to some external perturbation (e.g. a change in transmembrane potential).

The expression is used here simply to denote cases in which structural changes, rather than electron transfer, are rate limiting. The observed rates could be used to obtain structural and dynamic information on conformations of complexes, much like using Förster energy transfer to obtain structural information. Because the dependence of electron transfer rates on various parameters is much less well understood than energy transfer, however, rate observations will probably not provide definitive structural information (the same can often be said for energy transfer studies that are very useful for gross mapping of distances but provide little precise structural information). Liang et al (71, 72) also studied a series of complexes using various cytochromes that have different amino acid residues at the interface between the proteins in the putative complex. They observed significantly different rates of electron transfer and suggested an interpretation in which specific amino acid residues, especially aromatic residues, may enhance electron transfer rates. It appears, however, that these variations do not reflect differences in the electronic coupling matrix element but rather differences in complex structure or dynamics (B. Hoffmann, personal communication).

Ruthenated Proteins

The second class of proteins modified to examine electron transfer properties includes the extensive studies of Gray, his coworkers, and former coworkers (4, 6, 32, 39, 52, 62, 69, 73, 84a, 88, 94, 99, 112, 118, 122, 126, 127). They modified specific residues on proteins to study the transfer to or from redox centers inside the protein. The strategy of attaching a redox active metal to the protein avoids many of the problems encountered in loose complexes. Slowly interconverting conformations of the protein (especially near the surface) may change the distance. Cytochrome *c* has been modified by attaching ruthenium at a His residue 11.7 Å from the heme (His-edge to heme-edge) (39, 94, 112). By varying the central metal in the heme and the ligands on the Ru complex (aside from the His) and by studying reactions in both directions [Ru(II) → Fe(III) and Fe(II) → Ru(III)], a considerable range of driving forces has been obtained. The results demonstrate that the rate increases with increasing driving force and that the rate reaches a plateau when $-\Delta G_{et} \approx 1$–1.3 eV (94). Whether this plateau is actually the maximum in the rate vs free energy curve is not yet clear because the inverted region has not yet been sampled. Assuming that it is the maximum, the data can be reasonably well fit to a Marcus-type curve to give a reorganization energy of approximately 1.0–1.3 eV.

A significant extension of these experiments involves modification of amino acid residues that lie between the Ru on the surface and the heme group. Several possible pathways might be taken by the electron. The

pathway through peptide bonds between the Ru and heme is very long, so noncovalent electron transfer pathways seem more plausible. Various possibilities involving stretches of bonded pathways interrupted by small numbers of van der Waals contacts, hydrogen bonds, or salt bridges can be constructed. To evaluate such pathways, a hierarchy of values of the effectiveness of different types of bonded and nonbonded interactions is needed, and a first step in this direction has been outlined in a series of papers by Beratan and coworkers (7, 8, 31, 101). This approach is analogous to finding the paths of least resistance through a complex arrangement of circuits with different resistances at various points. By changing individual residues, the resistance associated with components in different pathways can, in principle, be varied. Because bonding pathways are expected to provide a much more significant electronic coupling than noncovalent pathways, we anticipate relatively few dominant pathways for typical proteins. Several cytochrome mutants have recently been prepared to test this model, but to date the observed rate of electron transfer and the predicted effects of specific changes is not definite (11). Since this work is still preliminary, we cannot rule out a significant role for specific pathways that might provide a fundamental mechanism for modulating electron transfer rates in proteins.

Cowan et al (31) have also modified sperm whale myoglobin by attaching ruthenium at surface histidines. Since several residues are accessible, several derivatives involving different distances, orientations relative to the heme group, and potential pathways through the protein are available. Ru-modified His-48 is 12.7 Å from the heme, and the rate, under conditions comparable with those described above for the modified cytochrome *c*, is about ten times slower. The researchers also modified other His residues 19.3, 20.1, and 22.0 Å from the heme. The rates for all these distances were somewhat more than two orders of magnitude slower than for His-48 (31). Thus, although the rate slows with distance, the decrease appears to attenuate much less at long distance than model systems predict (28). This result again raises the possibility that specific characteristics of the pathways between the donor and acceptor dominate the distance dependence, or that some process other than electron transfer is rate limiting. Studies of the dependence of the rate on driving force have also been presented for His-48 modified myoglobin, suggesting a reorganization energy of approximately 1.3 eV (31), which is comparable with other systems discussed above.

A few critical comments from the perspective of an investigator whose work has focussed primarily on the reaction center conclude this review. Studies of model protein systems generally lack references to studies of electron transfer in the RC, yet studies of electron transfer in the RC are

more extensive, both experimentally and theoretically, than in the model proteins. Significantly with the exception of the cytochrome *c*/cytochrome *c* peroxidase and cytochrome *c*/cytochrome b_5 systems, none of the model systems involves a protein-based donor-acceptor combination whose natural function is electron transfer, which is the business of the RC. Although it is not often stressed, the electron transfer reactions in many of the model protein systems are not fully reversible. This irreversibility presumably often results from the instability of the porphyrin cation radicals in the heme pocket. In contrast, the reactions discussed here for the RC are completely reversible at all temperatures equal to or lower than the physiological. Both forward and recombination rates have consequently been measured with much better signal-to-noise than for the model proteins. Until recently, one of the shortcomings of working with RCs was that the limited variations made systematic studies quite difficult. Quinone substitution experiments have now advanced to the point where a wide range of driving force in both the Q_A and Q_B sites can be investigated (46, 53, 54), electric fields can be used to manipulate various factors, and site-specific mutagenesis can be used to vary residues that may participate in electron transfer. Thus, the RC is becoming a model system in itself (11a) and comparisons with other model protein and nonprotein (28) electron transfer systems should be very useful.

ACKNOWLEDGMENTS

The work from the author's research group on the Stark effect and initial charge separation step was done by Dr. David J. Lockhart, the Stark effect studies of the heterodimer mutant by Sharon Hammes and Laura Mazzola, and the electromodulated $P^+Q_A^-$ recombination kinetics by Stefan Franzen and Robert Goldstein. More details of their work appear in the cited references. I am also very grateful to my collaborators, Drs. Holten, Kirmaier, and Schenck. I thank Drs. Scott, Beratan, Gray, and Hoffmann for helpful discussions and preprints. This work was supported by a grant from the National Science Foundation.

Literature Cited

1. Allen, J. P., Feher, G., Yeates, T. O., Komiya, H., Rees, D. C. 1987. *Proc. Natl. Acad. Sci. USA* 84: 5730–34
2. Allen, J. P., Feher, G., Yeates, T. O., Komiya, H., Rees, D. C. 1987. *Proc. Natl. Acad. Sci. USA* 84: 6162–66
3. Arata, H., Parson, W. W. 1981. *Biochim. Biophys. Acta* 636: 70–81
4. Axup, A. W., Albin, M., Mayo, S. L., Crutchley, R. J., Gray, H. B. 1988. *J. Am. Chem. Soc.* 110: 435–39
5. Barber, J. 1988. *Nature* 333: 114
6. Bechtold, R., Kuehn, C., Lepre, C., Isied, S. S. 1986. *Nature* 322: 286–88
7. Beratan, D. N., Onuchic, J. N. 1989. *Photosyn. Res.* In press
8. Beratan, D. N., Onuchic, J. N., Hop-

field, J. J. 1987. *J. Chem. Phys.* 86: 4488–98
9. Bixon, M., Jortner, J. 1988. *J. Phys. Chem.* 92: 7148–56
10. Bixon, M., Jortner, J., Michele-Beyerle, M., Ogrodnik, A., Lersch, W. 1987. *Chem. Phys. Lett.* 140: 622–30
11. Bowler, B. E., Meade, T. J., Mayo, S. L., Richards, J. H., Gray, H. B. 1989. *J. Inorg. Biochem.* 36: 210 (Abstr.)
12. Boxer, S. G., Chidsey, C. E. D., Roelofs, M. G. 1983. *Annu. Rev. Phys. Chem.* 34: 389–417
13. Boxer, S. G., Goldstein, R. A., Franzen, S. 1988. In *Photoinduced Electron Transfer*, ed. M. A. Fox, M. Chanon, 8: 163–215. Amsterdam: Elsevier
14. Boxer, S. G., Goldstein, R. A., Lockhart, D. J., Middendorf, T. R., Takiff, L. 1989. *J. Phys. Chem.* 93: 8280–94
15. Boxer, S. G., Lockhart, D. J., Franzen, S. 1989. In *Photochemical Energy Conversion*, ed. J. R. Norris Jr., D. Meisel, pp. 196–210. Amsterdam: Elsevier
16. Boxer, S. G., Lockhart, D. J., Kirmaier, C., Holten, D. 1989. *Perspectives in Photosynthesis*, ed. J. Jortner, B. Pullman. Amsterdam: Elsevier. In press
17. Boxer, S. G., Lockhart, D. J., Middendorf, T. R. 1987. *Springer Proc. Phys.* 20: 80–90
18. Braun, H. P., Michel-Beyerle, M. E., Breton, J., Buchanan, S., Michel, H. 1987. *FEBS Lett.* 221: 221–25
19. Breton, J., Martin, J.-L., Fleming, G. R., Lambry, J. C. 1988. *Biochemistry* 27: 8276–84
20. Breton, J., Martin, J.-L., Migus, A., Antonetti, A., Orszag, A. 1986. *Proc. Natl. Acad. Sci. USA* 83: 5121–25
20a. Budil, D. E., Gast, P., Chang, C.-H., Schiffer, M., Norris, J. R. 1987. *Annu. Rev. Phys. Chem.* 38: 561–83
21. Bylina, E. J., Kirmaier, C., McDowell, L., Holten, D., Youvan, D. C. 1988. *Nature* 336: 182–84
22. Bylina, E. J., Youvan, D. C. 1988. *Proc. Natl. Acad. Sci. USA* 85: 7226–30
23. Cave, R. J., Siders, P., Marcus, R. A. 1986. *J. Phys. Chem.* 90: 1436
24. Chang, C.-H., Tiede, D., Tang, J., Smith, U., Norris, J., Schiffer, M. 1986. *FEBS Lett.* 205: 82–86
25. Cheung, E., Taylor, K., Kornblatt, J. A., English, A. M., McLendon, G., Miller, J. R. 1986. *Proc. Natl. Acad. Sci. USA* 83: 1330–33
26. Chidsey, C. E. D., Kirmaier, C., Holten, D., Boxer, S. G. 1984. *Biochim. Biophys. Acta* 766: 424–37
27. Chidsey, C. E. D., Takiff, L., Goldstein, R. A., Boxer, S. G. 1985. *Proc. Natl. Acad. Sci. USA* 82: 6850–54
27a. Clayton, R. K., Yau, H. F. 1972. *Biophys. J.* 12: 867–81
28. Closs, G. L., Miller, J. R. 1988. *Science* 240: 440–46
28a. Coleman, W. J., Youvan, D. C. 1990. *Annu. Rev. Biophys. Biophys. Chem.* 19: 333–67
29. Conklin, K. T., McLendon, G. 1986. *Inorg. Chem.* 25: 4804–6
30. Conklin, K. T., McLendon, G. 1988. *J. Am. Chem. Soc.* 110: 3345–50
31. Cowan, J. A., Umpacis, R. K., Beratan, D. N., Onuchic, J. N., Gray, H. B. 1988. *Ann. NY Acad. Sci.* 550: 68–84
32. Crutchley, R. J., Ellis, W. R., Gray, H. B. 1985. *J. Am. Chem. Soc.* 107: 5002–4
33. Debus, R. J., Feher, G., Okamura, M. Y. 1985. *Biochemistry* 24: 2488–2500; 1986. 25: 2276–87
34. Deisenhofer, J., Epp, O., Miki, K., Huber, R., Michel, H. 1984. *J. Mol. Biol.* 180: 385–98
35. Deisenhofer, J., Epp, O., Miki, K., Huber, R., Michel, H. 1985. *Nature* 318: 618–24
36. DeLeeuv, D., Malley, M., Butterman, G., Okamura, M. Y., Feher, G. 1982. *Biophys. Soc. Abstr.* 37: 111a
36a. DeVault, D. 1984. *Quantum-Mechanical Tunneling in Biological Systems*. Cambridge: Cambridge Univ. Press. 2nd ed.
37. DiMagno, T., Angerhofer, A., Norris, J. R., Bylina, E. 1989. *Physiol. Plant* 76: A31 (Abstr.)
38. Ditson, S. L., Davis, R. C., Pearlstein, R. M. 1984. *Biochim. Biophys. Acta* 766: 623–29
39. Elias, H., Chou, M. H., Winkler, J. R. 1988. *J. Am. Chem. Soc.* 110: 429–34
40. Fajer, J., Brune, D. C., Davis, M. S., Forman, A., Spaulding, L. D. 1975. *Proc. Natl. Acad. Sci. USA* 72: 4956–60
41. Feher, G., Arno, T. R., Okamura, M. Y. 1988. In *The Photosynthetic Bacterial Reaction Center: Structure and Dynamics*, ed. J. Breton, A. Vermeglio, p. 271. New York: Plenum
42. Feher, G., Okamura, M. Y. 1978. In *The Photosynthetic Bacteria*, ed. R. K. Clayton, W. R. Sistrom, pp. 349–86. New York: Plenum
42a. Fischer, S. 1970. *J. Chem. Phys.* 53: 3195–3207
43. Fischer, S. F., Scherer, P. O. J. 1987. *Chem. Phys. Lett.* 115: 151–58
43a. Fleming, G. R., Martin, J.-L., Breton, J. 1988. *Nature* 333: 190

44. Franzen, S., Goldstein, R. F., Boxer, S. G. 1990. *J. Phys. Chem.* In press
45. Frauenfelder, H., Hartmann, H., Karplus, M., Kuntz, I. D. Jr., Kuriyan, J., et al. 1987. *Biochemistry* 26: 254
46. Giangiacomo, K. M., Dutton, P. L. 1989. *Proc. Natl. Acad. Sci. USA* 86: 2658–62
47. Gingrich, D. J., Nocek, J. M., Natan, M. J., Hoffman, B. M. 1987. *J. Am. Chem. Soc.* 109: 7533–34
48. Goldstein, R. A., Boxer, S. G. 1987. *Biophys. J.* 51: 937–46
49. Goldstein, R. A., Boxer, S. G. 1989. *Biochim. Biophys. Acta* 977: 70–77, 78–86
50. Goldstein, R. A., Takiff, L., Boxer, S. G. 1988. *Biochim. Biophys. Acta* 934: 253–63
51. Gopher, A., Schonfeld, M., Okamura, M. Y., Feher, G. 1985. *Biophys. J.* 48: 311–20
52. Gray, H. B. 1986. *Chem. Soc. Rev.* 15: 17–30
53. Gunner, M. R., Dutton, P. L. 1989. *J. Am. Chem. Soc.* 111: 3400–12
54. Gunner, M. R., Robertson, D. E., Dutton, P. L. 1986. *J. Phys. Chem.* 90: 3783–95
55. Hammes, S., Boxer, S. G. Submitted
56. Hammes, S. L., Mazzola, L., Boxer, S. G., Gaul, D. F., Schenck, C. C. 1990. *Proc. Natl. Acad. Sci. USA* In press
56a. Ho, P. S., Sutoris, C., Liang, N., Margoliash, E., Hoffman, B. M. 1985. *J. Am. Chem. Soc.* 107: 1070–71
57. Hochstrasser, R. 1973. *Acc. Chem. Res.* 6: 263–69
58. Hoff, A. J. 1986. *Photochem. Photobiol.* 43: 727–45
59. Hoffman, B. M., Ratner, M. A. 1987. *J. Am. Chem. Soc.* 109: 6237–43
60. Hoganson, C. W., Windsor, M. W., Farkas, D. I., Parson, W. W. 1987. *Biochim. Biophys. Acta* 892: 275
61. Holzapfel, W., Finkele, U., Kaiser, W., Oesterhelt, D., Scheer, H., et al. 1989. *Chem. Phys. Lett.* 160: 1–7
62. Isied, S. S., Kuehn, C., Worosila, G. 1984. *J. Am. Chem. Soc.* 106: 1722–26
62a. Jortner, J. 1976. *J. Chem. Phys.* 64: 4860–67
63. Kaufmann, K. J., Dutton, P. L., Netzel, T. L., Leigh, J. S., Rentzepis, P. M. 1975. *Science* 188: 1301–4
64. Kirmaier, C., Bylina, E. J., Youvan, D. C., Holten, D. 1989. *Chem. Phys. Lett.* 159: 251–57
65. Kirmaier, C., Holten, D. 1987. *Photosynth. Res.* 13: 225–60
66. Kirmaier, C., Holten, D. 1988. *FEBS Lett.* 239: 211–18
67. Kirmaier, C., Holten, D., Bylina, E. J., Youvan, D. C. 1988. *Proc. Natl. Acad. Sci. USA* 85: 7562–66
68. Kleinfeld, D., Okamura, M. Y., Feher, G. 1984. *Biochemistry* 23: 5780–86
69. Kostic, N. M., Margalit, R., Che, C.-M., Gray, H. B. 1983. *J. Am. Chem. Soc.* 105: 7765–67
70. Kuki, A., Boxer, S. G. 1983. *Biochemistry* 22: 2923–33
70a. Levich, V. G., Dogonadze, R. R. 1959. *Dokl. Akad. Nauk SSSR* 124: 123–26
71. Liang, N., Kang, C. H., Ho, P. S., Margoliash, E., Hoffman, B. M. 1986. *J. Am. Chem. Soc.* 108: 4665–66
72. Liang, N., Mauk, A. G., Pielak, G. J., Johnson, J. A., Smith, M., Hoffman, B. M. 1988. *Science* 240: 311–13
73. Lieber, C. M., Karas, J. L., Gray, H. B. 1987. *J. Am. Chem. Soc.* 109: 3778–79
74. Liptay, W. 1974. In *Excited States*, ed. E. C. Lim, 1: 129–229. New York: Academic
75. Lockhart, D. J., Boxer, S. G. 1987. *Biochemistry* 26: 664 68, 2958
76. Lockhart, D. J., Boxer, S. G. 1988. *Proc. Natl. Acad. Sci. USA* 85: 107–11
77. Lockhart, D. J., Boxer, S. G. 1988. *Chem. Phys. Lett.* 144: 243
78. Lockhart, D. J., Goldstein, R. F., Boxer, S. G. 1988. *J. Chem. Phys.* 89: 1408–15
79. Lockhart, D. J., Kirmaier, C., Holten, D., Boxer, S. G. 1989. *J. Phys. Chem.* Submitted
80. Lösche, M., Feher, G., Okamura, M. Y. 1987. *Proc. Natl. Acad. Sci. USA* 84: 7537
81. Lösche, M., Feher, G., Okamura, M. Y. 1988. See Ref. 42, pp. 151–64
82. Marcus, R. A. 1956. *J. Chem. Phys.* 24: 966–78
82a. Marcus, R. A. 1965. *J. Chem. Phys.* 43: 679 701
83. Marcus, R. A., Sutin, N. 1985. *Biochim. Biophys. Acta* 811: 265–322
84. Margalit, R., Kostic, N. M., Che, C.-M., Blair, D. F., Chiang, H.-J., et al. 1984. *Proc. Natl. Acad. Sci. USA* 81: 6554–58
84a. Margalit, R., Pecht, I., Gray, H. B. 1983. *J. Am. Chem. Soc.* 105: 301–2
85. Martin, J. L., Breton, J., Hoff, A. J., Migus, A., Antonetti, A. 1986. *Proc. Natl. Acad. Sci. USA* 83: 957–61
86. Mathies, R. A. 1974. *Experimental and theoretical studies on the excited electronic states of some aromatic hydrocarbons through electric field perturbation.* PhD dissertation. Cornell Univ., Ithaca, NY
87. Mathies, R. A., Stryer, L. 1976. *Proc. Natl. Acad. Sci. USA* 73: 2169

88. Mayo, S. L., Ellis, W. R., Crutchley, R. J., Gray, H. B. 1986. *Science* 233: 948–52
89. McGourty, J. L., Blough, N. V., Hoffman, B. M. 1983. *J. Am. Chem. Soc.* 105: 4470–72
90. McGourty, J. L., Peterson-Kennedy, S. E., Ruo, W. Y., Hoffman, B. M. 1987. *Biochemistry* 26: 8302–12
91. McLendon, G., Guarr, T., McGuire, M., Simolo, K., Strauch, S., Taylor, K. 1985. *Coord. Chem. Rev.* 64: 113–24
92. McLendon, G., Miller, J. R. 1985. *J. Am. Chem. Soc.* 107: 7811–16
93. McLendon, G., Pardue, K., Bak, P. 1987. *J. Am. Chem. Soc.* 109: 7540–41
94. Meade, T. J., Gray, H. B., Winkler, J. R. 1989. *J. Am. Chem. Soc.* 111: 4353–56
95. Michel, H., Epp, O., Deisenhofer, J. 1986. *EMBO J.* 5: 2445–51
96. Michel-Beyerle, M. E., Plato, M., Deisenhofer, J., Michel, H., Bixon, M., Jortner, J. 1988. *Biochim. Biophys. Acta* 932: 52–70
97. Mikkelsen, K. V., Ulstrup, J., Zakaraya, M. G. 1989. *J. Am. Chem. Soc.* 111: 1315–19
98. Moog, R. S., Kuki, A., Fayer, M. D., Boxer, S. G. 1984. *Biochemistry* 23: 1564–71
99. Nocera, D. G., Winkler, J. R., Yocom, K. M., Bordignon, E., Gray, H. B. 1984. *J. Am. Chem. Soc.* 106: 5145–50
100. Okamura, M. Y., Feher, G. 1986. *Proc. Natl. Acad. Sci. USA* 83: 8152–56
101. Onuchic, J. N., Beratan, D. N. 1987. *J. Am. Chem. Soc.* 109: 6771–78
102. Parot, P., Thiery, J., Vermeglio, A. 1987. *Biochim. Biophys. Acta* 893: 534–43
103. Parson, W. W., Warshel, A. 1987. *J. Am. Chem. Soc.* 109: 6152–63
104. Peterson-Kennedy, S. E., McGourty, J. L., Ho, P. S., Sutoris, C. J., Liang, N., et al. 1985. *Coord. Chem. Rev.* 64: 125–33
105. Peterson-Kennedy, S. E., McGourty, J. L., Hoffman, B. M. 1984. *J. Am. Chem. Soc.* 106: 5010–12
106. Plato, M., Möbius, K., Michel-Beyerle, M. E., Bixon, M., Jortner, J. 1988. *J. Am. Chem. Soc.* 110: 7279–85
107. Popovic, Z. D., Kovacs, G. J., Vincett, P. S., Alegria, G., Dutton, P. L. 1986. *Chem. Phys.* 110: 227–37
108. Popovic, Z. D., Kovacs, G. J., Vincett, P. S., Alegria, G., Dutton, P. L. 1986. *Biochim. Biophys. Acta* 851: 38–48
109. Popovic, Z. D., Kovacs, G. J., Vincett, P. S., Dutton, P. L. 1985. *Chem. Phys. Lett.* 116: 405–10
110. Poulos, T. L., Finzel, B. 1984. *Peptide Protein Rev.* 4: 115–79
111. Rockley, M. G., Windsor, M. W., Cogdell, R. J., Parson, W. W. 1975. *Proc. Natl. Acad. Sci. USA* 72: 2251–55
111a. Sarai, A. 1979. *Chem. Phys. Lett.* 63: 360–66
112. Schenck, C., Gaul, D., Cummings, B. Submitted
113. Sebban, P., Wraight, C. A. 1989. *Biochim. Biophys. Acta* 974: 54–65
114. Shuvalov, V. A., Amesz, J., Duysens, L. N. M. 1986. *Biochim. Biophys. Acta* 851: 327
115. Shuvalov, V. A., Klevanik, A. V. 1983. *FEBS Lett.* 160: 51
116. Simolo, K. P., McLendon, G. L., Mauk, M. R., Mauk, A. G. 1984. *J. Am. Chem. Soc.* 106: 5012–13
117. Steffen, M., Boxer, S. G. 1989. *FEBS Lett.* Submitted
118. Toi, H., Mar, G. N. L., Margalit, R., Che, C.-M., Gray, H. B. 1984. *J. Am. Chem. Soc.* 106: 6213–17
119. Ulstrup, J. 1979. *Charge Transfer Processes in Condensed Media.* Berlin: Springer-Verlag
120. Warshel, A., Creighton, S., Parson, W. W. 1988. *J. Phys. Chem.* 92: 2697–2701
121. Windsor, M. W. 1988. See Ref. 41, p. 289
122. Winkler, J. R., Nocera, D. G., Yocom, K. M., Bordingnon, E., Gray, H. B. 1982. *J. Am. Chem. Soc.* 104: 5798–5800
123. Won, Y., Friesner, R. A. 1988. *Biochim. Biophys. Acta* 935: 9–18
124. Woodbury, N. W., Becker, M., Middendorf, D., Parson, W. W. 1985. *Biochemistry* 24: 7516–21
125. Woodbury, N. W., Parson, W. W. 1984. *Biochim. Biophys. Acta* 767: 345–61
125a. Woodbury, N. W., Parson, W. W., Gunner, M. R., Prince, R. C., Dutton, P. L. 1986. *Biochim. Biophys. Acta* 851: 6–22
126. Yocom, K. M., Shelton, J. B., Shelton, J. R., Schroeder, W. A., Worosila, G., et al. 1982. *Proc. Natl. Acad. Sci. USA* 79: 7052–55
127. Yocom, K. M., Winkler, J. R., Nocera, D. G., Bordignon, E., Gray, H. B. 1983. *Chem. Scr.* 21: 29–33
128. Zankel, K. L., Reed, D. W., Clayton, R. K. 1968. *Proc. Natl. Acad. Sci. USA* 61: 1243